Article

Single–molecule Level Quantification Reveals the Interaction between Melittin and Lipopolysaccharide by Atomic Force Microscopy

Sheng Huang , Guoqi Su , Li Yang , Liangguang Yue , Li Chen , Jinxiu Huang * , Feiyun Yang *

Posted Date: 30 August 2024

doi: 10.20944/preprints202408.2140.v1

Keywords: melittin; lipopolysaccharide; atomic force microscopy; interaction force; kinetics characteristics

 doi:10.20944/preprints202408.2140.v1

Article

Single−Molecule Level Quantification Reveals the Interaction between Melittin and Lipopolysaccharide by Atomic Force Microscopy

Sheng Huang [1,2], Guoqi Su [1,2], Li Yang [2], Liangguang Yue [2], Li Chen [1,2], Jinxiu Huang [1,2,*] and Feiyun Yang [1,2,*]

[1] Animal Nutrition Institute, Chongqing Academy of Animal Science, Chongqing, China
[2] Institute of Nutrition and Feed, National Center of Technology Innovation for Pigs, Chongqing, China
* Correspondence: huangjx@cqaa.cn (J.H.); yfeiyun@yeah.net (F.Y.)

Abstract: The interaction forces and mechanical properties of the interaction between melittin (Mel) and lipopolysaccharide (LPS) are considered a crucial driving force for Mel in killing Gram−negative bacteria (GNB). However, how their interaction forces are performed at the single−molecule level and the dissociation kinetic characteristics of the Mel/LPS complex remain poorly understood. In this study, the single−molecule level interaction forces between Mel and LPSs from *E. coil* K−12, O55:B5, O111:B4, and O128:B12 were explored using atomic force microscopy (AFM) based single−molecule force spectroscopy (SMFS). Further, the AFM−based dynamic force spectroscopy (DFS) and advanced analytical model were employed to investigate the kinetic characteristics of the Mel/LPSs complex dissociation. The results indicated that Mel could interact with both rough (R)−form LPS (*E. coli* K−12) and smooth (S)−form LPSs (*E. coli* O55:B5, O111:B4, O128:B12), and the S−form LPSs showed a more robust interaction with Mel than R−form LPS, and a slight difference existed in the interaction forces between Mel and diverse S−form LPSs. The Mel interacts with S−form LPSs showed greater specific and non−specific interaction forces than R−form LPS ($p < 0.05$), as determined by AFM−based SMFS. However, there was no significant difference in the specific and non−specific interaction forces among the three S−form LPSs ($p > 0.05$), indicating the variability of O−antigen could not affect the interaction between Mel and LPSs. The DFS result showed that the Mel/S−form LPSs complexes had a lower dissociation rate constant (k_{off}), a shorter energy barrier width (x_β), a longer bond lifetime (τ_{off}), and a higher height of the energy barrier (ΔG), demonstrating that Mel could interact with S−form LPSs to form more stable complexes. In conclusion, this study promotes our knowledge of the interaction micromechanics and kinetics characteristics between Mel and LPS at the single−molecule level. Moreover, it can help us design and evaluate new anti−GNB drugs.

Keywords: melittin; lipopolysaccharide; atomic force microscopy; interaction force; kinetics characteristics

1. Introduction

Gram−negative bacteria (GNB), especially multidrug−resistant *E. coli* infection, is exponentially increasing, posing one of the most urgent global healthcare and economic threats[1]. These Gram−negative species have a structurally dynamic cell envelope, enabling them to resist multiple antibiotics[2]. However, the new treatment ideas have not been sufficient, and antimicrobial resistance continues to escalate, acting as a global ticking time bomb. There is an urgent need to develop new therapies to manage GNB infections and reduce the occurrence of bacterial resistance through new antibacterial drugs.

GNB is classified by their multi−layered macromolecular structure on the cell envelope, consisting of three components: the outer membrane (OM), the peptidoglycan layer, and the inner membrane (IM) (shown in Figure 1)[3]. The OM is a crucial component of GNB, protecting the bacteria from extreme external environments and acting as a barrier to arrest the entry of harmful compounds [4].

 doi:10.20944/preprints202408.2140.v1

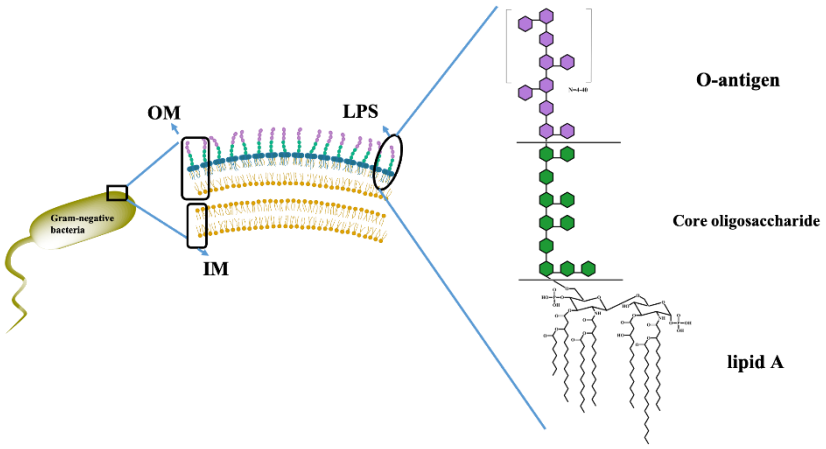

Figure 1. Schematic diagram of the cell membrane structure of GNB.

LPS is a critical component of the OM that maintains the structure and permeability of GNB[5]. LPS strongly interact with each other through bridging by divalent cations, which bind the negatively charged phosphate groups of lipid A−core, avoiding repulsion and maintaining OM integrity[6]. Since LPS is the barrier to mediate the entry of antimicrobials, it has been increasingly recognized as a critical component in determining antimicrobial susceptibility and the target for antibacterial drug development.

Antimicrobial peptides (AMPs) are promising antimicrobial reagents that combat the ongoing global threat of multidrug−resistant bacteria[7]. It is extensively agreed that AMPs kill bacteria via a membrane−lytic mechanism[8]. The membrane−targeted mode of action often leads to rapid killing. However, AMPs must first interact with and penetrate the LPS before reaching the cytoplasm of the GNB[9]. Therefore, LPS is the foremost site of interaction with the AMP.

Melittin (Mel) is a significant AMP in bee venom, and multiple in vitro studies have found that it has substantial antimicrobial activity against GNB[10,11]. Our previous research found that Mel showed a rapid bactericidal effect by interacting with LPS and penetrating the bacterial OM and IM of *E. coli* ATCC 25922[12]. Brand et al. showed that Mel interacts with an OM model of GNB, increasing the membrane permeability and decreasing OM stability when bound to Mel[13]. Structural and thermodynamic research indicated that Mel binding to LPS was an endothermic process, and Mel's helical conformation and C−terminus could be the significant factor in recognizing LPS[14]. However, the above studies are based on a conventional bulk scale and cannot clarify the single−pair biomechanical interaction between Mel and LPS at the micro or nanoscale. A more profound, single−molecule level quantificadtion of the interactions between Mel and LPS can help to elaborate Mel's mechanism of antimicrobial activity and to develop new anti−GNB drugs based on Mel in the future.

Atomic force microscopy (AFM) has been regarded as a potent method for quantifying biomolecular interaction at the nanoscale level[15]. Sun et al. used AFM to reveal the interaction force between pro−apoptotic protein (BAX) and B−cell lymphoma 2 (Bcl−2). The result showed complex non-covalent interactions at the BAX/Bcl-2 through AFM−based single−molecule force spectroscopy (SMFS)[16]. Another study used AFM to evaluate the interaction forces between LPS and monoclonal antibodies (mAbs), and the result indicated that a single bond between LPS and mAbs included a non-specific component along with an immunochemically specific one[17]. Previously, we probed the change in calcium ion (Ca^{2+})−induced interaction forces between Mel and calmodulin by AFM[18]. The result indicated that the unbinding force between Mel and calmodulin increased in the presence of Ca^{2+} in a concentration−dependent manner.

This study used AFM to quantitatively describe the interactions between Mel and LPSs at the single−molecule level. The appropriate analysis model determined the contribution of non−covalent bonds to Mel/LPS interaction. We also portrayed the dissociation kinetic characteristics of the Mel/LPSs complex through AFM−based DFS. The results provide new insight into the biomechanical

 doi:10.20944/preprints202408.2140.v1

information of LPS/Mel interaction and present a novel approach to exploring the bactericidal mechanism of Mel.

2. Results and Discussion

2.1. Morphological Characterization of LPSs from Different E. coli

LPS is a significant glycolipid substance composed of three structural domains: lipid A, core oligosaccharide(Core OS), and the O−antigen(Figure 2)[19,20]. The overall structure of LPS is conserved, and the lipid A structure is conserved at the species level. Meanwhile, the Core OS vary among species and even between some strains of one species. The most diverse component of LPS is the O−antigen. Not only do the structure and composition differ within a species at the strain level, leading to a high number of serotypes of E. coli[21], but some Gram−negative bacteria do not even synthesize O−antigen. The molecules composed of only lipid A and the Core OS are typically referred to as "rough(R) form" LPS, as opposed to "smooth(S) form" LPS, which includes the O−antigen[22]. The LPSs from E. coli O55:B5, O111:B4, and O128:B12 used in this study were typical S−form LPSs, and the LPS from E. coli K−12 was R−form LPS.

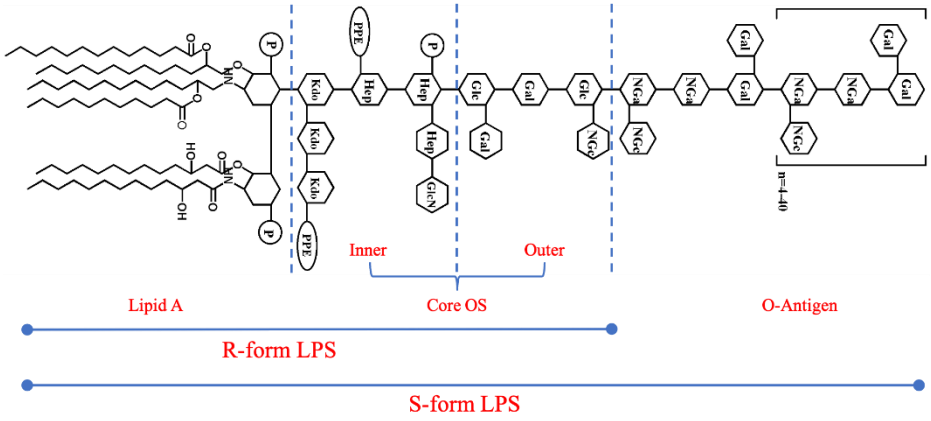

Figure 2. The chemical structure of LPS. Abbreviations: Kdo, 3−deoxy−α−Dmanno−oct−2−ulopyranosonic acid; PPE: phosphatidyl ethanolamine; Hep: heptose; Glc: glucose; Gal: galactose; NGc: glucosamine; NGa: galactosamine; P, phosphate. R: Rough; S: Smooth.

In this work, LPSs immobilised onto the mica surface were implemented using a COOH−NH_2 linking way, and the non−contact mode of AFM was used as an efficient technology to reveal the nanoscale surface morphology of mica and LPSs. The surface of the fresh mica was smooth and burr−free (Figure 3A); nevertheless, the LPS molecules were evenly distributed, and most of the imaged LPS particles were nanosized aggregates (Figure 3B−E).

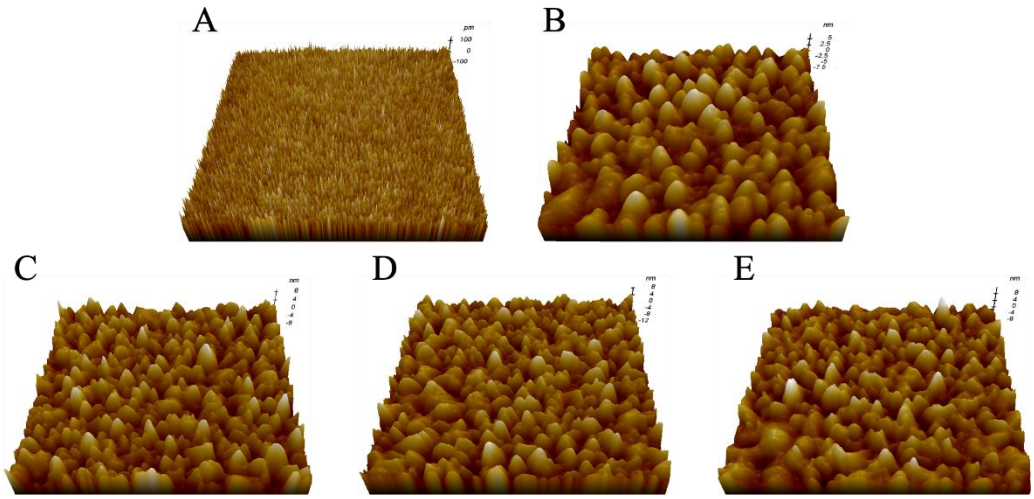

 doi:10.20944/preprints202408.2140.v1

Figure 3. AFM was imaging the 3D-topography surface of mica and LPSs from different *E. coils*. (A) Mica, (B) LPS from *E. coli* K−12, (C) LPS from *E. coli* O55:B5, (D) LPS from *E. coli* O111:B4, (E) LPS from *E. coli* O128:B12. The samples were scanned using a line frequency of 1 Hz with a resolution of 512 × 512 pixels and a scanning size of 1 × 1 μm.

The surface morphology of mica and LPSs was analysed using XEI software to characterise the surface morphology characteristics quantitatively. The average roughness (Ra) and average height (μ) were used to describe the surface properties of mica and LPSs (Table 1). The results revealed that the average roughness of fresh mica was 0.057 ± 0.003 nm² with an average height of 0.231 ± 0.004 nm, indicating mica has a very smooth surface. After covalent linking LPS from E. coli K−12 onto the mica surface, the surface average roughness was significantly increased to 0.216 ± 0.004 nm² with an average height of 13.245 ± 0.071 nm, indicating that the distribution of LPS was single−layered and prone to assemble on a surface in bundles.

Table 1. Average roughness (Ra) and average height (μ) of the mica and LPSs.

No.	Sample	Parameter	
		Ra, nm²	μ, nm
1	Mica	0.057 ± 0.003	0.231 ± 0.004
2	LPS from *E. coli* K-12	0.216 ± 0.004	13.245 ± 0.071
3	LPS from *E. coli* O55:B5	0.304 ± 0.002	17.352 ± 0.045
4	LPS from *E. coli* O111:B4	0.335 ± 0.007	18.106 ± 0.062
5	LPS from *E. coli* O128:B12	0.315 ± 0.011	17.566 ± 0.051

As shown in Table 1, when the LPSs from E. coli O55:B5, O111:B4, and O128:B12 anchored onto mica, the average roughness and average height of the three LPSs did not show significant differences. However, compared to the LPS from E. coli K−12, the average roughness and height of the three LPSs significantly improved. This result is consistent with the previous description[17]. The O−antigen portion of LPSs from E. coli O55:B5, O111:B4, and O128:B12 have a long hydrophilic chain. As AFM imaging was operated in the air, less water in the hydrophilic chain made the hydrophilic chain more close. This kind of hydration causes the surface of LPSs from E. coli O55:B5, O111:B4, and O128:B12 to show a higher average roughness and average height than LPS from E. coli K−12. However, hydration less impacted LPS from E. coli K−12 because it lacks the O−antigen portion[23]. The experimental results indicated that LPSs can be successfully anchored on the surface of mica by COOH−NH_2 linking way, which lays a foundation for the subsequent mechanical detection.

2.2. Probing the Interaction Forces between Mel and LPSs

This study focused on investigating the single−molecule interaction force between Mel and LPSs. However, in a homogenous solution, it is hard to dynamically study the interact biomechanics between Mel and LPSs unless they were fixed to a matrix surface. Hence, we used a self−assembled monolayer (SAM) method to fix the Mel onto the gold−modified AFM probe surface, as described before[18]. The LPSs were anchored onto the mica surface following the process from Ananchenko et al. [17]. The detection of interaction forces between Mel and LPSs was promoted using AFM-based SMFS.

The force−distance curves were recorded after the Mel−modified probes were moved to the site on the surface of the LPSs surface and retracted to the initial set point. When the probes approach the set point of the surface of LPSs and are pulled away from the binding point, the probes will be deflected due to the interaction forces between Mel and LPSs, and the instrument could detect a "force−displacement" curve. A typical operation process and the force−distance curve between Mel and LPSs is shown in Figure 4.

Preprints.org (www.preprints.org) | NOT PEER-REVIEWED | Posted: 30 August 2024 doi:10.20944/preprints202408.2140.v1

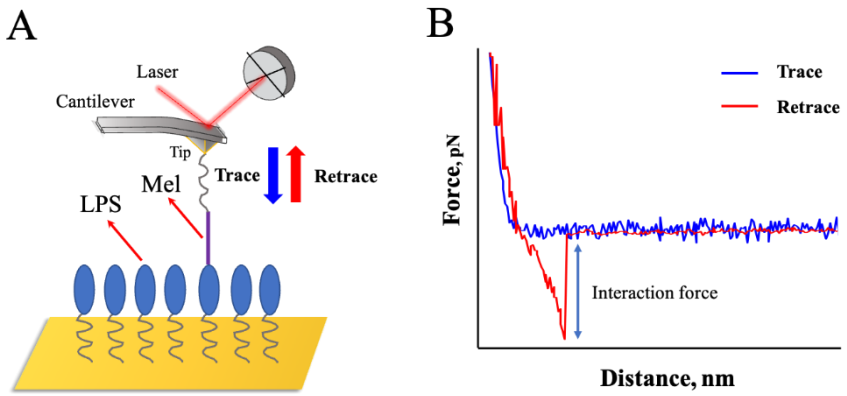

Figure 4. The detection of adhesion forces between Mel and LPSs using AFM−based SMFS. (A) The principle of the experimental process. An AFM probe functionalized with Mel was approached and retracted from a mica surface functionalized with LPSs. (B) A representative force−distance curve shows the force data obtained using the AFM.

Here, the AFM probes can be regarded as an elastic material. The deflection of the probes was converted to the force (F) according to Hooke's law, as follows:

$$F = k \times \Delta z \quad (1)$$

Where Δz is the deflection of the probes, and k is the spring constant of the probes.

During the interaction forces measurement, the binding of Mel and LPSs is random, and the interaction forces did not occur in each measurement because of the electrostatic interaction between probes and mica[24]. The interaction forces between Mel and LPSs were measured several hundred times to overcome this limitation. The force histograms were drawn with approximately 300 force measurements for each Mel and LPS group, and the possible interaction forces were fitted with the Gaussian distribution shown in Figure 5.

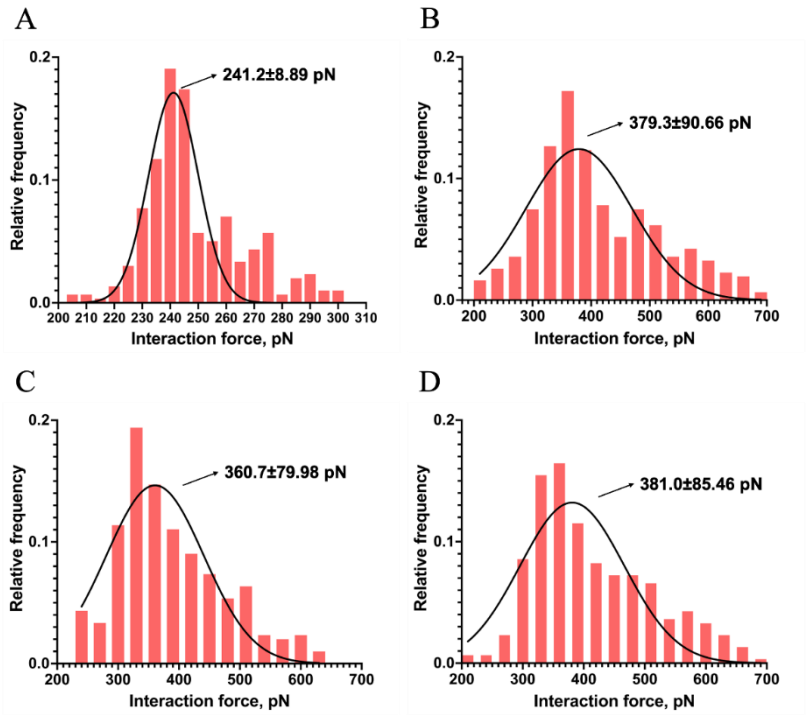

Figure 5. Interaction force−frequency distribution histograms with Gaussian fitting curves between Mel and LPSs from *E. coli* K−12 (A), *E. coli* O55:B5 (B), O111:B4 (C), and O128:B12 (D), respectively.

 doi:10.20944/preprints202408.2140.v1

As shown in Figure 5, the maximum interaction force between Mel and LPS from *E. coli* K−12 appeared at 241.2 ± 8.89 pN (Figure 5A). While the maximum interaction forces between Mel and LPS from *E. coli* O55:B5, O111:B4, and O128:B12 occurred at 379.3 ± 90.66, 360.7 ± 79.98, 381.0 ± 85.46 pN (Figure 5B−D), respectively. The results indicated that Mel could interact with both R−form LPS (*E. coli* K−12) and S−form LPSs (*E. coli* O55:B5, O111:B4, O128:B12), and the S−form LPSs showed a greater interact with Mel than R−form LPS. However, slight differences existed in the interaction forces between Mel and diverse S−form LPSs. The results suggested that both polysaccharide and lipid A structures of LPS contribute to the interaction between Mel and LPSs.

2.3. Investigation of Single−Molecule Interaction Between Mel and LPSs

The results of the interaction forces obtained during the force AFM detection reflected the interaction between multiple pairs of Mel and LPS due to the AFM probe tip having a certain radius of curvature, which agreed with the previous study[18]. To explore the interaction between a single pair of Mel and LPSs, the Poisson statistical analysis method was used to analyze the measured interaction forces[25,26]. Before proceeding with the analysis, it should be assumed that in a given area, the total interaction forces measured by AFM consisted of a finite distribution of the number of interacting bonds, which was subject to a Poisson distribution. The specific interaction force (F) could derive to specific interaction force (F_i) and non−specific interaction force (F_0) of a single pair Mel−LPS.

The F measured from an actual AFM measurement is related to the bond break number (n) in a single trace and retrace event:

$$F=nF_i \quad (2)$$

In the equation, *F is* indicated as the mean value of a single bond−breaking force and is expected as a constant value.

The variance (σ_m^2) and mean (μ_m) value of the interaction forces were acquired by detecting multiple trace and retrace events. Due to the relationship between measured interaction forces and the break bond number, the following formula was given:

$$\mu_m=\mu_n F_i \quad (3)$$

$$\sigma_m^2=\sigma_n^2 F_i^2 \quad (4)$$

Further, the single−pair interaction force (F_i) can be calculated as the following formula:

$$F_i=\frac{\sigma_m^2}{\mu_m} \quad (5)$$

When considering the possible non−specific interaction force (F_0), the above formula was changed to:

$$\mu_m=\mu_n F_i+F_0 \quad (6)$$

$$\sigma_m^2=\sigma_n^2 F_i^2=\mu_m F_i-F_i F_0 \quad (7)$$

According to the Poisson distribution model, the specific interaction force (F_i) and the non−specific interaction force (F_0) between a single pair of Mel−LPS can be calculated by the following equation:

$$\sigma_m^2=\mu_m F_i-F_i F_0 \quad (8)$$

Where, σ_m^2 and μ_m are referred to variance and mean value of the detected interaction forces.

The total interaction forces between Mel and LPSs by measuring 50~60 repeats at each of 6 randomly chosen points of LPSs surface. The variance (σ_m^2) and mean (μ_m) value of the approximately 300 times force measurement were calculated, and the linear fitting of the variance plotted versus the

 doi:10.20944/preprints202408.2140.v1

mean was shown in Figure 6. The slope and the intercept value of the obtained regression curve were the F_i and the F_iF_0 of the single molecule pair of Mel and LPS, respectively.

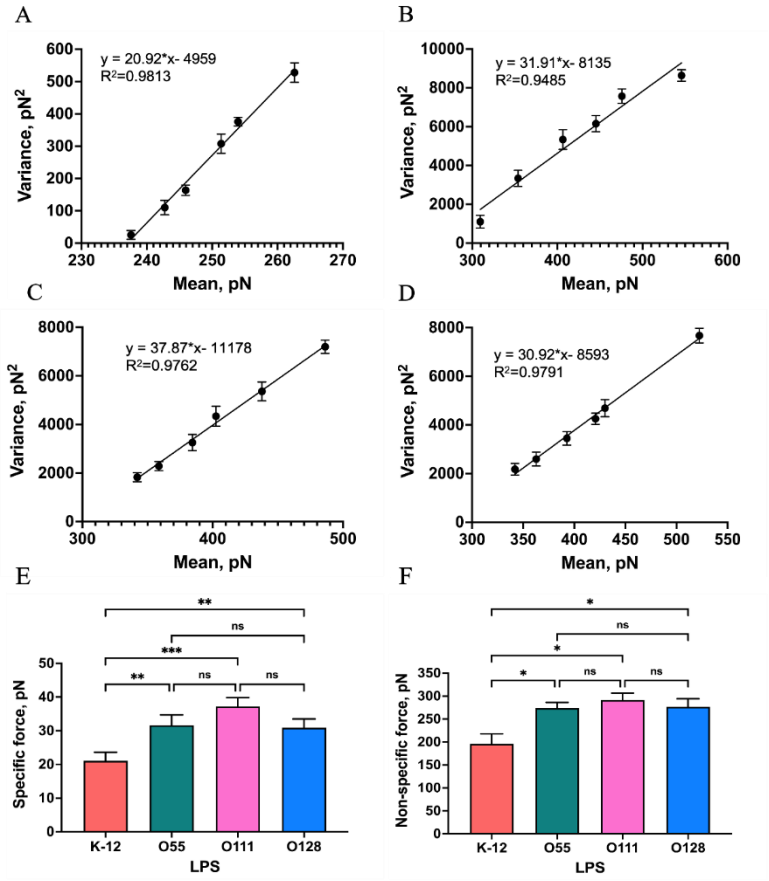

Figure 6. Measurement of single−molecule specific and non−specific interaction between Mel and LPSs. (A−D) linear relationship of the mean plotted versus the variance of the interaction force between Mel and LPS from *E. coli* K−12, O55:B5, O111:B4, and O128:B12, respectively. (E, F) The specific (E) and non−specific (F) interaction forces between a single pair of Mel and LPSs (ns: no significance, * indicates *p*−values < 0.05, ** indicates *p*−values < 0.01, *** indicates *p*−values < 0.001 on ordinary one-way ANOVA).

Earlier study has addressed the role of LPS in regulating the interaction with AMPs. The O−antigen of LPS could bind to organic molecules by electrostatic and hydrogen bonding[27]. Wen et al. indicated that electrostatic interaction could regulate the AMP−LPS vesicle interaction[28]. Joshua et al. suggested that the interaction between immobilized AMPs and deliquescent LPS molecules occurs at the lipid A portion by electrostatic attraction and hydrophobic interactions[29]. A molecular dynamics simulation study revealed that the Gly1 residue in the N−terminus of Mel interacts with the phosphate group in lipid A by formatting the hydrogen bonds[9]. The above studies indicated that hydrogen bonding, hydrophobic and electrostatic interactions play crucial roles in the interaction between AMP and LPS. In the Poisson distribution analysis, the chemical and hydrogen bonds contribute to the specific interaction, whereas the electrostatic and hydrophobic interactions are included in non−specific interaction. This study resolved the specific and non−specific forces between single pair Mel and LPSs by Poisson distribution. As shown in Figure 6 E and F, the specific interaction forces between Mel and LPSs from *E. coli* K−12, O55:B5, O111:B4, and O128:B12 were 21.1 ± 2.08, 31.7 ± 2.51 37.2 ± 2.14, and 30.9 ± 2.07 pN, while, the non−specific interaction forces were 196.3 ± 30.59, 273.9 ± 17.6, 291.4 ± 21.29, and 276.8 ± 24.62 pN, respectively. These results indicated that Mel could bind to LPS from *E. coli* K−12 by hydrogen bonds, electrostatic attraction and hydrophobic interaction, which simultaneously showed the specific and non−specific interaction forces. In addition, Mel interacts with S−form LPSs showed greater specific and non-specific

 doi:10.20944/preprints202408.2140.v1

interaction forces than R−form LPS ($p < 0.05$), due to the existence of O−antigen (Figure 6E, 6F). It can also be seen that there was no significant difference in the specific and non−specific interaction force among three S−form LPSs ($p > 0.05$), which proved that the presence of O−antigen could promote the interaction between Mel and LPS, and the O−antigen variability could not affect the interaction between Mel and LPS. Therefore, it could be speculated that in the process of LPS binding, Mel first generated hydrogen bond and electrostatic interaction with the O−antigen, and then, the amino acids of Mel bound with the lipid A by hydrogen bonds, electrostatic interaction, and hydrophobic interaction.

2.4. Quantitatively Probing the Kinetic Characteristics of the Mel/LPSs Dissociation

Our study showed that Mel and LPSs from different *E. coli* display strong interaction, but there were some differences. We then explored whether these diversities stem from the dissociation process of the Mel/LPS complex using DFS−based AFM. The dissociation kinetic characteristics between Mel and LPSs can be conducted and extracted by varying the loading rate and recording the interaction forces during the DFS experiments[30].

Furthermore, the Bell−Evans model (Figure 7) was used to express the relationship between the interaction force(F) and the logarithm of the loading rate (r):

$$F=\frac{k_BT}{x_\beta}In\left(\frac{rx_\beta}{k_{off}k_BT}\right) \quad (9)$$

F is the most probable interaction force, k_B is Boltzmann's constant, T is the absolute temperature, x_β is the energy barrier width, r is the loading rate, and k_{off} is the dissociation rate constant.

In addition, the bond lifetime (τ_{off}) of single pair Mel and LPS binding is the inverse form of the dissociation rate constant (k_{off}), which is:

$$\tau_{off}=\frac{1}{k_{off}} \quad (10)$$

In the experiment, the force−distance curves were gathered under a gradient increasing loading rate, and the most probable interaction forces confirmed by Gaussian distribution were plotted against the loading rate on a log scale (Figure 8).

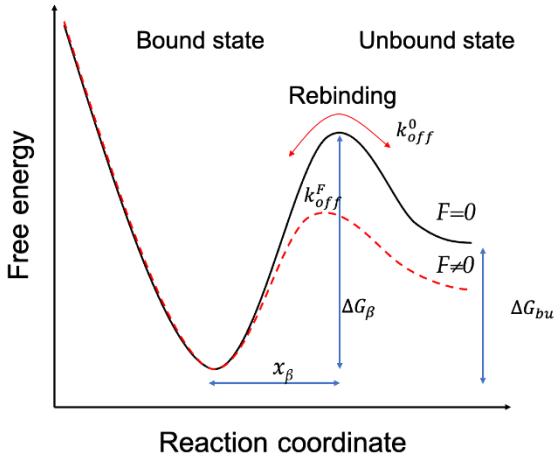

Figure 7. A schematic diagram of the energy landscape, depending on external forces. The Bell−Evans model described a Mel−LPS bond as a two-state model. The bound state is separated from the unbound state by a single energy barrier located at a distance (x_β).

 doi:10.20944/preprints202408.2140.v1

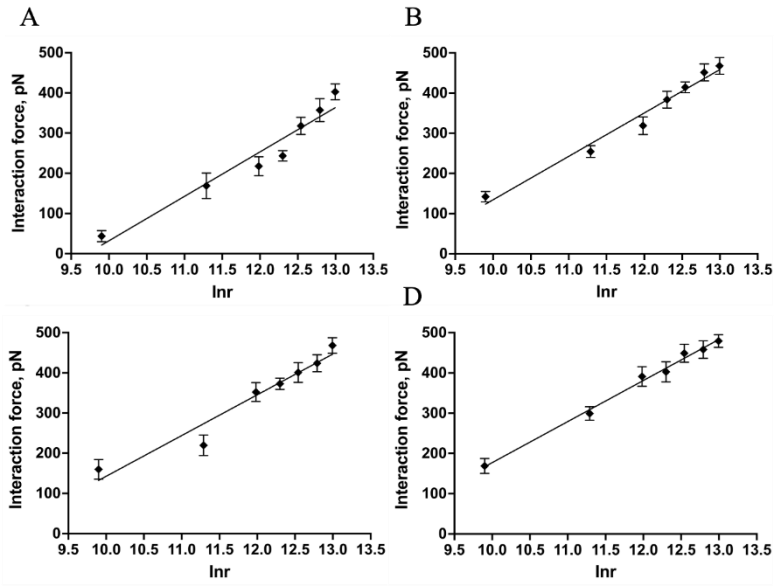

Figure 8. Probing the kinetic characteristics of the Mel/LPSs Dissociation. DFS plot showing the distribution of the interaction forces as a function of their LR measured between the Mel and LPSs from *E. coli* K−12 (A), O55:B5 (B), O111:B4 (C), and O128:B12(D), respectively.

Several AFM-based DFS studies have shown that the interaction between biological macromolecules is related to the intrinsic interaction and the loading rates. Using DFS, it is possible to transform the mechanics information to the thermodynamic and kinetic parameters[31–33]. Detecting the most probable interaction forces at various loading rates can reveal the dissociation dynamics of the Mel-LPSs interaction. The results showed that the most probable interaction forces as a function of the loading rate exhibit only one regression curve (Figure 8), the same as in earlier studies[34,35], meaning that the binding complex of Mel/LPSs follows a simple two−state model, which the bound state is separated from the unbound state by a single energy barrier[36]. Once the k_{off} has been obtained, the height of the energy barrier, ΔG can be deduced using the following equation:

$$\Delta G = -k_B T In \frac{k_{off} h}{k_B T} \quad (11)$$

Where h is Planck's constant and $k_B T$ is the thermal energy.

As shown in Table 2, the values of the dissociation rate constant (k_{off}) were 110.91 ± 5.51, 108.04 ± 4.27, 99.82 ± 5.57, and 101.44 ± 3.54 S^{-1} for Mel and LPSs from *E. coli* K−12, O55:B5, O111:B4, and O128:B12 respectively. Compared with the k_{off} value of Mel/R−LPS, the k_{off} values of three Mel/S−LPSs were smaller, which demonstrated that the Mel and S−LPSs interaction was stronger than Mel and R−LPS, probably owing to the lower stability of Mel/R−LPS complex. The values of the energy barrier width (x_β) for Mel and LPSs from *E. coli* K−12, O55:B5, O111:B4, and O128:B12 were 0.1052 ± 0.0018, 0.9464 ± 0.0028, 0.8717 ± 0.0031, and 0.8427 ± 0.0031 nm, respectively. The energy barrier widths, $\boldsymbol{x_\beta}$, were shorter for Mel/S−LPSs than Mel/R−LPS, which indicated that the energy landscape was described by a narrower energy valley[37], and could be described as less conformational variability[38]. Meanwhile, the bond lifetime (τ_{off}) values of single pair of Mel/LPS binding were 9.038 ± 0.448, 9.271 ± 0.371, 10.005 ± 0.574, and 9.870 ± 0.349 ms, respectively. The single pair Mel/R−LPS bond lifetime (τ_{off}) was shorter than Mel/S−LPSs, which indicated a high affinity and stability of the Mel/S−LPSs complex with a longer lifetime for high−affinity interactions. In addition, the height of the energy barrier (ΔG) values for Mel and LPSs from *E. coli* K−12, O55:B5, O111:B4, and O128:B12 were 24.748 ± 0.049, 24.774 ± 0.040, 24.854 ± 0.056, and 24.837 ± 0.035 $k_B T$, respectively. The calculation of the energy barrier height showed that the ΔG value of Mel and S−LPSs were higher than Mel and R−LPS, suggesting that the Mel/S-LPSs complexes were more challenging to dissociate than Mel and R−LPS[37].

 doi:10.20944/preprints202408.2140.v1

Table 2. The kinetic and energy landscape parameters of the Mel/LPSs dissociation.

Sample	K_{off}, S^{-1}	x_β, nm	τ_{off}, ms	ΔG, k_BT
LPS from E. coli K-12	110.91 ± 5.51	0.10517 ± 0.0018	9.038 ± 0.448	24.748 ± 0.049
LPS from E. coli O55:B5	108.04 ± 4.27	0.09464 ± 0.0003	9.271 ± 0.371	24.774 ± 0.040
LPS from E. coli O111:B4	99.82 ± 5.57	0.08717 ± 0.0003	10.005 ± 0.574	24.854 ± 0.056
LPS from E. coli O128:B12	101.44 ± 3.54	0.08427 ± 0.0003	9.870 ± 0.349	24.837 ± 0.035

3. Materials and Methods

3.1. Materials and Reagents

N−hydroxysuccinimide (NHS), N−(3−dimethylaminopropyl)−N−ethylcarbodiimide hydrochloride (EDC), 16−mercaptohexadecanoic acid (MHA) were purchased from Sigma−Aldrich (Sigma−Aldrich Shanghai Trading Co. Ltd, Shanghai, China). LPSs from *E. coli* O55:B5, *E. coli* O111:B4, *E. coli* O128:B12, and *E. coli* K−12 were purchased from Sigma−Aldrich (Sigma−Aldrich Shanghai Trading Co Ltd, Shanghai, China). Melittin was purchased from Yuanye (Shanghai Yuanye Bio−Technology Co. Ltd, Shanghai, China). (3-aminopropyl)triethoxysilane (APTES), triethylamine and ethanolamine were purchased from Macklin (Shanghai Macklin Biochemical Technology Co., Ltd., Shanghai, China). AFM probes (OMCL−AC240TS and PPP−CONTCSAu) were purchased from Olympus (Olympus Corporation, Tokyo, Japan) and Nanosensors (NANOSENSORS, Neuchatel, Switzerland). Gold−coated silicon substrates and mica were purchased from Ted Pella (Ted Pella, INC., Redding, CA, USA). Deionized water (18.25 MΩ·cm) was obtained in−house using a Direct−Q 3 Millipore Ultrapure water purification system (Millipore, Burlington, MA, USA).

3.2. Immobilization of Mel on Gold−Coated AFM Probes

The immobilization of Mel on the gold−coated AFM probes was implemented as previously described with a simple modification[18]. Briefly, gold−coated AFM probes (PPP−CONTCSAu with tip radius < 50 nm, resonance frequency of 25 kHz and the standard spring constant of 0.2 N/m) were UV−radiated for 15 min to remove contamination from a surface. After cleaning, the probes were immersed into 1 mM MHA ethanolic solution for 24 h at room temperature, followed by washing with ethanol and drying with nitrogen. Subsequently, the MHA−modified probes were immersed in a mixture solution of NHS (10 mg/mL) and EDC (25 mg/mL) and incubated for 30 min at room temperature to activate terminal carboxyl groups. Finally, the treated probes were inserted into Mel solution (10 μg/mL in PBS) and incubated overnight at 4 °C. The remaining activated carboxyl groups were deactivated with 1 M ethanolamine. After washing with PBS, the Mel-functionalized probes were used to measure force spectroscopy.

3.3. Immobilization of LPSs on Mica

A previously described method with a modification was followed for functionalizing LPSs onto micas[17]. Firstly, the vacuum desiccator was filled with argon, and freshly cleaved micas were put inside. Then, 30 μL APTES and 10 μL triethylamine were put into a vacuum desiccator for mica−amination within 1.5 h. The aminopropyl−modified micas were used for further immobilization of LPSs. A mixture of PBS solution of NHS (final concentration 10 mg/mL) and EDC (final concentration 25 mg/mL) was added sequentially to LPSs (final concentration 10 μg/mL) PBS solution. The mixture was stored for 1 min, and then the aminopropyl−modified micas were immersed in this solution. After 2 h incubation, the micas were washed thoroughly with PBS for subsequent morphological imaging and force spectroscopy measurement.

3.4. Interaction Force Measurements between Mel and LPSs

The adhesion forces between Mel and LPSs were measured using Park System NX−10 atomic force microscopy (Park System Co., Suwon, Korea). The Mel−functionalized AFM probes were first

 doi:10.20944/preprints202408.2140.v1

scanned across the LPSs monolayer and bare mica (as blank control) at a randomly selected location. Then, force measurements were taken with the Mel−functionalized probes moved toward the desired point of the surface of the LPSs and retracted back to the initial point. When the probes were approaching the monolayer surface and then retracted away from the binding point, it was deflected due to the Mel−LPS interaction force, which was detected on the instrument as a "voltage−displacement" signal, followed by its transformation into a "force−displacement" curve. In this study, Mel−modified probes were used in all the force experiments, and the spring constant was calibrated using the thermal fluctuation method.

All interaction forces measurements between Mel and LPSs were performed using contact mode at 25 °C. Several hundred force curves were collected: 3 experiments (~300 force curves per set) were conducted on 3 different samples using 3 probes. The velocity of the probe during retracement was set to 1000 nm/s. Interaction forces were calculated and analyzed from the collected "force−displacement" curves using the XEI processing software program (Park System Co., Suwon, Korea). Six locations in the LPS monolayer were randomly selected. Measurements were taken approximately 50 to 60 times at each point to obtain a more accurate statistical analysis. The LPSs−free mica was used as the control group. The block study was conducted by measuring the interaction forces in the presence of free Mel in a PBS solution.

3.5. Dynamic Force Spectrum Measurements between Mel and LPSs

AFM−based DFS measured the interaction forces to estimate the dissociation kinetic parameters between Mel and LPSs. Briefly, the interaction forces between Mel and LPSs were measured under the same approaching velocity of 1000 nm/s and variable retraction velocity range from 100 to 2200 nm/s, with a threshold force of 500 pN, and probe contact time remained at 0.6 s. All samples were run at least three times. All force curves were analyzed using the XEI processing software program (Park System Co., Suwon, Korea).

3.6. Morphological Characterization of LPSs

All morphological images of LPSs were obtained using Park System NX-10 atomic force microscopy (Park System Co., Suwon, Korea). The AFM imaging study was performed at a scan rate of 0.5~1 Hz, with the image resolution set to 512 × 512. Briefly, AFM was performed in a non−contact mode in air employing a scanning size of 1 × 1 μm. Images of the LPSs and the roughness of surfaces were collected and analyzed using the XEI processing software program (provided by the manufacturer).

3.7. Data Analysis

Statistical analysis was performed using the software GraphPad Prism 10. Force data are shown as the mean with standard deviation (SD) from at least three independent experiments. Statistical significance was analyzed using a one-way ANOVA. Statistical differences are expressed as *** $p < 0.0001$, ** $p < 0.001$, and * $p < 0.005$.

5. Conclusions

This study used the AFM-based SMFS and DFS methods to quantify and reveal the interaction between Mel and LPSs on a single−molecule level. The interaction forces between Mel and LPSs were detected by approximating the Mel-modified probes to the LPS monolayer and then retreating to the set original position. We found that Mel could interact with both R−form LPS and S−form LPSs, and the S−form LPSs showed a stronger interaction with Mel than R-form LPS. Furthermore, a Poisson statistical analysis method was used to analyze the specific and non−specific interaction forces between Mel and LPSs at a single−molecule level. The results shown that Mel interacts with S−form LPSs showed greater specific and non−specific interaction forces than R−form LPS due to the existence of O−antigen, demonstrating that in the process of LPS binding, Mel could interact with the O−antigen by generating the hydrogen bond and electrostatic attraction, and then, the amino acids

 doi:10.20944/preprints202408.2140.v1

of Mel bound with the lipid A by hydrogen bonds, electrostatic attraction, and hydrophobic interaction. We also explored the dissociation process of the Mel/LPS complex using DFS−based AFM to reveal the reason for the variation of the interaction forces between Mel and different LPSs. By the Bell-Evans model analyzed, the complex formed by Mel and S−form LPSs had a shorter energy barrier width and a smaller dissociation rate constant during the dissociation process, which indicated that Mel could form a more stable complex after interacting with S−form LPSs. In summary, this research may complement the traditional rules for screening AMPs and elucidate the antibacterial mechanism, which provides an exciting insight into the use of AFM.

Author Contributions: Data curation, Sheng Huang and Liangguang Yue; Formal analysis, Li Yang and Li Chen; Writing – original draft, Sheng Huang and Guoqi Su; Writing – review & editing, Jinxiu Huang and Feiyun Yang. All authors have read and agreed to the published version of the manuscript.

Funding: This research was financed from the following funds: Chongqing Natural Science Foundation General Project (CSTC2021jcyj—msxmX0807), Special Project for Performance Incentive and Guidance of Research Institutions in Chongqing (17437).

Institutional Review Board Statement: Not applicable.

Informed Consent Statement: Not applicable.

Data Availability Statement: Data are contained within the article.

Conflicts of Interest: The authors declare no conflicts of interest.

References

1. Doi, Y.; Bonomo, R.A.; Hooper, D.C.; Kaye, K.S.; Johnson, J.R.; Clancy, C.J.; Thaden, J.T.; Stryjewski, M.E.; van Duin, D. Gram-negative bacterial infections: research priorities, accomplishments, and future directions of the antibacterial resistance leadership group. *Clin Infect Dis* **2017**, *64*, S30-S35, doi:10.1093/cid/ciw829.
2. Sun, J.; Rutherford, S.T.; Silhavy, T.J.; Huang, K.C. Physical properties of the bacterial outer membrane. *Nat Rev Microbiol* **2022**, *20*, 236-248, doi:10.1038/s41579-021-00638-0.
3. Impey, R.E.; Hawkins, D.A.; Sutton, J.M.; Soares da Costa, T.P. Overcoming intrinsic and acquired resistance mechanisms associated with the cell wall of gram-negative bacteria. *Antibiotics* **2020**, *9*, 623.
4. Saxena, D.; Maitra, R.; Bormon, R.; Czekanska, M.; Meiers, J.; Titz, A.; Verma, S.; Chopra, S. Tackling the outer membrane: facilitating compound entry into Gram−negative bacterial pathogens. *npj Antimicrob Resist* **2023**, *1*, 17.
5. Sperandeo, P.; Martorana, A.M.; Zaccaria, M.; Polissi, A. Targeting the LPS export pathway for the development of novel therapeutics. *BBA−Mol Cell Res* **2023**, *1870*, 119406.
6. Romano, K.; Hung, D. Targeting LPS biosynthesis and transport in gram-negative bacteria in the era of multi−drug resistance. *BBA−Mol Cell Res* **2023**, *1870*, 119407.
7. Chen, N.; Jiang, C. Antimicrobial peptides: Structure, mechanism, and modification. *Eur J Med Chem* **2023**, *255*, 115377.
8. Espeche, J.C.; Varas, R.; Maturana, P.; Cutro, A.C.; Maffía, P.C.; Hollmann, A. Membrane permeability and antimicrobial peptides: Much more than just making a hole. *Peptide Sci* **2024**, *116*, e24305.
9. Stephani, J.C.; Gerhards, L.; Khairalla, B.; Solov'yov, I.A.; Brand, I. How do antimicrobial peptides interact with the outer membrane of Gram-negative bacteria? role of lipopolysaccharides in peptide binding, anchoring, and penetration. *ACS Infect. Dis.* **2024**, 10, 763–778.
10. Lima, W.G.; de Lima, M.E. Therapeutic Prospection of animal venoms-derived antimicrobial peptides against infections by multidrug−resistant acinetobacter baumannii: A systematic review of pre−clinical studies. *Toxins* **2023**, *15*, 268.
11. Gong, H.; Hu, X.; Zhang, L.; Fa, K.; Liao, M.; Liu, H.; Fragneto, G.; Campana, M.; Lu, J.R. How do antimicrobial peptides disrupt the lipopolysaccharide membrane leaflet of Gram-negative bacteria? *J Colloid Interf Sci* **2023**, *637*, 182-192.
12. Huang, S.; Su, G.; Jiang, S.; Chen, L.; Huang, J.; Yang, F. New N−terminal fatty−acid−modified melittin analogs with potent biological activity. *Int J Mol Sci* **2024**, *25*, 867.
13. Brand, I.; Khairalla, B. Structural changes in the model of the outer cell membrane of Gram−negative bacteria interacting with melittin: an in situ spectroelectrochemical study. *Faraday Discuss* **2021**, *232*, 68-85.
14. Bhunia, A.; Domadia, P.N.; Bhattacharjya, S. Structural and thermodynamic analyses of the interaction between melittin and lipopolysaccharide. *BBA−Biomembranes* **2007**, *1768*, 3282-3291.

15. Lostao, A.; Lim, K.; Pallarés, M.C.; Ptak, A.; Marcuello, C. Recent advances in sensing the inter−biomolecular interactions at the nanoscale−A comprehensive review of AFM-based force spectroscopy. *Int J Biol Macromol* **2023**, 124089.
16. Sun, H.; Tian, Y.; Fu, Y.; Lei, Y.; Wang, Y.; Yan, X.; Wang, J. Single-molecule scale quantification reveals interactions underlying protein-protein interface: from forces to non-covalent bonds. *Phys Chem Chem Phys* **2023**, *25*, 31791-31803, doi:10.1039/d3cp04351g.
17. Ananchenko, B.; Belozerov, V.; Byvalov, A.; Konyshev, I.; Korzhavina, A.; Dudina, L. Evaluation of intermolecular forces between lipopolysaccharides and monoclonal antibodies using atomic force microscopy. *Int J Biol Macromol* **2020**, *156*, 841-850, doi:10.1016/j.ijbiomac.2020.04.055.
18. Huang, S.; Wang, J.; Sun, H.; Fu, Y.; Wang, Y. Probing changes in Ca2+-induced interaction forces between calmodulin and melittin by atomic force microscopy. *Micromachines* **2020**, *11*, 906.
19. Sabnis, A.; Edwards, A.M. Lipopolysaccharide as an antibiotic target. *BBA−Mol Cell Res* **2023**, *1870*, 119507.
20. Di Lorenzo, F.; Duda, K.A.; Lanzetta, R.; Silipo, A.; De Castro, C.; Molinaro, A. A journey from structure to function of bacterial lipopolysaccharides. *Chem. Rev.* **2021**, *122*, 15767-15821.
21. Golomidova, A.; Naumenko, O.; Senchenkova, S.; Knirel, Y.; Letarov, A. The O−polysaccharide of Escherichia coli F5, which is structurally related to that of E. coli O28ab, provides cells only weak protection against bacteriophage attack. *Arch Virol* **2019**, *164*, 2783-2787.
22. Raetz, C.R.; Whitfield, C. Lipopolysaccharide endotoxins. *Annu Rev Biochem* **2002**, *71*, 635-700.
23. Lu, Q.; Wang, J.; Faghihnejad, A.; Zeng, H.; Liu, Y. Understanding the molecular interactions of lipopolysaccharides during E. coli initial adhesion with a surface forces apparatus. *Soft Matter* **2011**, *7*, 9366-9379.
24. Zhou, Y.; Cao, W.; Xu, Z.; Zhang, X.F.; Liu, Y. Binding kinetics of liposome conjugated E−selectin and P−selectin glycoprotein ligand-1 measured with atomic force microscopy. *Colloid Surface B* **2021**, *207*, 112002.
25. Jiang, Y.; Zhu, C.; Ling, L.; Wan, L.; Fang, X.; Bai, C. Specific aptamer−protein interaction studied by atomic force microscopy. *Anal. Chem.* **2003**, *75*, 2112-2116.
26. Lo, Y.S.; Huefner, N.D.; Chan, W.S.; Stevens, F.; Harris, J.M.; Beebe, T.P. Specific interactions between biotin and avidin studied by atomic force microscopy using the Poisson statistical analysis method. *Langmuir* **1999**, *15*, 1373-1382.
27. Jucker, B.; Harms, H.; Hug, S.; Zehnder, A. Adsorption of bacterial surface polysaccharides on mineral oxides is mediated by hydrogen bonds. *Colloid Surface B* **1997**, *9*, 331-343.
28. Guo, W.; Xu, S.; Reichart, T.M.; Xiao, M.; Lu, T.; Mello, C.; Chen, Z. Probing molecular interactions between surface−immobilized antimicrobial peptides and lipopolysaccharides in situ. *Langmuir* **2020**, *36*, 12383-12393.
29. Uzarski, J.R.; Mello, C.M. Detection and classification of related lipopolysaccharides via a small array of immobilized antimicrobial peptides. *Anal. Chem.* **2012**, *84*, 7359-7366.
30. Yang, B.; Liu, Z.; Liu, H.; Nash, M.A. Next generation methods for single−molecule force spectroscopy on polyproteins and receptor-ligand complexes. *Front Mol Biosci* **2020**, *7*, 85.
31. Yang, J.; Petitjean, S.J.; Koehler, M.; Zhang, Q.; Dumitru, A.C.; Chen, W.; Derclaye, S.; Vincent, S.P.; Soumillion, P.; Alsteens, D. Molecular interaction and inhibition of SARS−CoV−2 binding to the ACE2 receptor. *Nat Commun* **2020**, *11*, 4541.
32. Fu, Y.; Wang, J.; Wang, Y.; Sun, H. Investigating the effect of tyrosine kinase inhibitors on the interaction between human serum albumin by atomic force microscopy. *Biomolecules* **2022**, *12*, 819.
33. Bizzarri, A.R.; Cannistraro, S. The application of atomic force spectroscopy to the study of biological complexes undergoing a biorecognition process. *Chem Soc Rev* **2010**, *39*, 734-749.
34. Akhunzada, M.J.; Yoon, H.J.; Deb, I.; Braka, A.; Wu, S. Bell-Evans model and steered molecular dynamics in uncovering the dissociation kinetics of ligands targeting G−protein−coupled receptors. *Sci Rep−UK* **2022**, *12*, 15972.
35. Rico-Pasto, M.; Zaltron, A.; Ritort, F. Force dependence of proteins' transition state position and the Bell–Evans model. *Nanomaterials* **2021**, *11*, 3023.
36. Wang, C.; Jin, Y.; Desai, U.R.; Yadavalli, V.K. Investigation of the heparin−thrombin interaction by dynamic force spectroscopy. *BBA-Gen Subjects* **2015**, *1850*, 1099-1106.
37. Qin, J.; Zhang, M.; Guan, Y.; Guo, X.; Li, Z.; Rankl, C.; Tang, J. Imaging and quantifying analysis the binding behavior of PD−L1 at molecular resolution by atomic force microscopy. *Anal Chim Acta* **2022**, *1191*, 339281.
38. Müller, D.J.; Dumitru, A.C.; Lo Giudice, C.; Gaub, H.E.; Hinterdorfer, P.; Hummer, G.; De Yoreo, J.J.; Dufrêne, Y.F.; Alsteens, D. Atomic force microscopy−based force spectroscopy and multiparametric imaging of biomolecular and cellular systems. *Chem. Rev.* **2020**, *121*, 11701-11725.

 doi:10.20944/preprints202408.2140.v1

disclaim responsibility for any injury to people or property resulting from any ideas, methods, instructions or products referred to in the content.